Effects of realistic band structures on the interlayer coupling strengths in magnetic multilayers

Byungchan Lee and Yia-Chung Chang
Department of Physics and Materials Research Laboratory, University of Illinois at Urbana-Champaign, 1110 West Green Street, Urbana, Illinois 61801-3080
(Received 2 March 1995)

The interlayer coupling strengths associated with different oscillation periods in Co/Cu/Co sandwiches for different orientations are calculated based on the spin-asymmetry of the reflection amplitude at extremal points. A realistic tight-binding model which includes s, p^3, and d^5 orbitals is adopted to calculate the reflection amplitudes. At the interface, all evanescent states are included to meet proper boundary conditions. The spin asymmetry of the reflection amplitude which is the crucial factor for determining the coupling strength is found to depend on the details of the band structures. Unique features are found when there are more than one reflected waves, which do not exist in the single-band model. For certain periods inferred from the spacer Fermi surface, the coupling strengths are found too small to be detected.

I. INTRODUCTION

The discovery of the exchange coupling between ferromagnetic layers separated by nonmagnetic spacer layers has stimulated a great deal of interest lately.[1,2] The relation between the period of the oscillatory coupling and the Fermi surface of the spacer material seems to be established to some degree. Theoretical studies indicate that the period is determined from the extremal spanning vector of the Fermi surface of the spacer material.[3,4] Experimentally, the change of period depending on the structure[5] or the orientation[6] was observed with the Cu spacer. The Fermi surface can be artificially altered in the Cu-Ni alloy and the increase of the oscillation period as a function of the composition was observed.[7–9] When the spacer is thin, the period can deviate from the spanning vector. Thus, observation of many oscillations up to a very thick spacer layer is necessary to measure the period accurately. Actually, Unguris *et al.* observed the interlayer coupling up to more than 50 monolayers (ML) of Ag (Ref. 10) and Au (Ref. 11) spacer and periods obtained from these experimental data are in good agreement with those predicted from the spanning vectors of the Fermi surface for the spacer materials. However, for transition-metal spacers, it is not well understood why only a few distinctive periods are observed experimentally among many possible periods inferred from the Fermi surface of the spacer.[12] Short periods can be suppressed by the sample condition such as the interface roughness.[13] However, in many cases even the possible long periods were not observed. In Fe/Cr multilayers, it is not clear yet which extremal or nesting feature of the Cr Fermi surface gives the experimentally observed long period.[14–16] Before comparing with the experimental data, one should examine the coupling strength for each possible period. The existence of the spanning vector in the spacer Fermi surface is the necessary but not sufficient condition. When the coupling strength corresponding to that period is too small, the period will not be observed experimentally.

Due to the spin splitting in the magnetic layer, electrons with different spins in the spacer layer "see" different boundary conditions at the interface. This causes a change of the density of states in the spacer and the interlayer coupling energy is the total-energy difference of the ferromagnetic and antiferromagnetic configurations. In first order, this can be calculated from the "force theorem."[17] Then, the interlayer coupling is the difference of the single-particle energies calculated with the single-particle Green's function and the T-matrix formalism. This method is applicable with the first-principles calculations[18–20] and also the interlayer coupling can be expressed in terms of the reflection amplitudes as shown by Bruno[21] and Stiles.[12] As commonly adopted in other theoretical models, perfect lattice match and sharp interfaces are assumed. The in-plane momentum $\mathbf{k}_{\|}$ is conserved throughout the multilayer and thus a good quantum number. In order to calculate the coupling strength, summation over $\mathbf{k}_{\|}$ needs to be performed and in the limit of a thick spacer, only the contribution near the extremal points of the Fermi surface is important. This suggests that in order to investigate the dependence of the coupling strength on material parameters and orientation, one should carefully examine how electron states associated with the extremal points match at the interface. This is expressed in terms of the spin asymmetry of the reflection amplitude at the extremal point, which is another factor for the coupling strength apart from the shape of the spacer Fermi surface. A similar argument was made based on the misalignment between the bands in the spacer and ferromagnetic layers by Mathon, Villeret, and Edwards.[22] Bruno evaluated the reflection amplitude with an s-like single-band tight-binding (TB) model for the (100) fcc Co/Cu/Co system but the sp-d band hybridization effects and evanescent states are not included.[21] In this paper, we present a realistic TB

method to calculate the reflection amplitude and examine the effects of *sp-d* hybridization on the coupling strength in Co/Cu/Co sandwiches for (001), (110), and (111) orientations. We will show that it is essential to take into account the *sp-d* hybridization and realistic band structures. When there are more than one reflected wave, the reflection amplitude will depend on how each reflected wave couples with the incident wave. The reflected wave which couples most strongly with the incident wave tends to get the predominant portion of the reflection. The results will be compared with other calculations and available experiments.

II. THEORETICAL MODEL

We consider a sandwich system which consists of two semi-infinite magnetic layers labeled by L (left) and R (right), separated by a nonmagnetic layer. The interlayer coupling J is defined as

$$J = \frac{\Omega_{\rm F} - \Omega_{\rm AF}}{2S}, \tag{1}$$

where $\Omega_{\rm F}$ and $\Omega_{\rm AF}$ are the grand canonical potentials for the ferromagnetic (F) and antiferromagnetic (AF) configurations and S is the area of the layer. Using the force theorem or the frozen potential approximation, the change in the grand potential $\Delta\Omega$ is given by the change in the single-particle density of states as[19–21]

$$\Delta\Omega_\nu = \frac{1}{\pi}{\rm Im}\sum_{\mathbf{k}_\parallel}\int_{-\infty}^{+\infty} d\varepsilon f(\varepsilon)\ {\rm Tr}\ \ln(1 - G_0\, T^{L,\nu} G_0\, T^{R,\nu}), \tag{2}$$

where ν labels the two coupling configurations (F and AF), G_0 is the unperturbed Green's function of the spacer material, T is the T matrix, f is the Fermi-Dirac distribution, and Tr denotes the trace. The interlayer coupling can be expressed in terms of reflection amplitudes as in Refs. 12 and 21. In this paper, a realistic multiband model is considered and in general there are many reflected waves. When the thickness D of the spacer is large, the dominant contribution comes from the extremal points and its asymptotic form (keeping only the leading term) can be shown to be (see Appendix A for details)

$$J = {\rm Im}\sum_\alpha \sum_{ij} \frac{\hbar v_{ij}^\alpha \kappa_{ij}^\alpha}{4\pi^2 D^2}\ (\Delta r_{ij}^\alpha)^2 e^{i(q_{ij}^\alpha D + \phi_{ij}^\alpha)} F_{ij}^\alpha(D,T)\ \theta_{ij}, \tag{3}$$

where

$$F_{ij}^\alpha(D,T) = \frac{2\pi k_{\rm B} T D/\hbar v_{ij}^\alpha}{\sinh(2\pi k_{\rm B} T D/\hbar v_{ij}^\alpha)}. \tag{4}$$

Here the superscript α is a label for different $\mathbf{k}_\parallel^\alpha$'s which are the in-plane projections of the extremal points on the Fermi surface. For a given $\mathbf{k}_\parallel^\alpha$, there can be several spanning vectors, denoted by $q_{ij} = k_i - k_j$, where k_i is the wave vector for the incoming wave and k_j is the wave vector for the reflected wave. Δr_{ij} is the spin asymmetry of the reflection amplitude, i.e., $\Delta r_{ij} = (r_{ij}^+ - r_{ij}^-)/2$, where r_{ij}^+ (r_{ij}^-) is the reflection amplitude for a majority (minority) spin associated with k_i and k_j. θ_{ij} is a constraint function, which takes the value 1 when q_{ij} is an extremal spanning vector and 0 otherwise. v_{ij}^α is the average group velocity at extremal points $\mathbf{k}_\parallel^\alpha + k_i\hat{z}$ and $\mathbf{k}_\parallel^\alpha + k_j\hat{z}$. κ_{ij}^α is the average curvature radius of the Fermi surface at the corresponding extremal points and the phase factor $\phi_{ij}^\alpha = 0$, $\pi/2$, and π for maxima, saddle points, and minima, respectively (see Refs. 12 and 21 for details).[23] The temperature-dependent factor $F_{ij}^\alpha(D,T)$ was tested in a recent experiment.[24] The coupling strength decreases at higher temperatures. In this paper, we only consider the zero-temperature case ($T = 0$). Then the coupling strength for a given period with n equivalent extremal spanning vectors is given by

$$I_0 |\Delta r_{ij}^\alpha|^2 / D^2, \tag{5}$$

where $I_0 = \hbar v_{ij}^\alpha \kappa_{ij}^\alpha n/4\pi^2$ which is determined by the geometry of the spacer Fermi surface. In this paper, the reflection amplitudes are calculated from the realistic TB model with s, p^3, and d^5 orbitals. The method is described in Appendix B. We express the eigenstate of the heterostructure using the complex-band solutions[25] of each material including the evanescent states. By imposing proper boundary conditions at the interface, we can obtain the reflection and transmission amplitudes.

III. fcc Co/Cu/Co SANDWICHES

In this section, we apply the method of Sec. II to Co/Cu/Co sandwiches. The thickness of each Co layer is assumed to be semi-infinite. The TB parameters for Cu are taken from Ref. 26 with the p on-site energy (E_p) adjusted slightly to make the Fermi surface closer to the de Haas–van Alphen measurements.[27] The best fit E_p is found to be 1.366 51 Ry and the resulting Fermi surface is shown in Fig. 1 together with experimental data from Ref. 27. Also shown in the figure are the extremal spanning vectors (q_{ij}^α). For fcc Co, we take parameters of paramagnetic Co from Ref. 26 and adjust on-site energies E_s, E_p, E_d for each spin by fitting the band structure to that in Ref. 28. The best-fit on-site energies for both spins are listed in Table I. In both materials, $E = 0$ is taken as the Fermi level. The lattice constant of Cu is $a = 3.603$ Å (Ref. 27) and it is assumed to be the same for Co. We calculate the strength of the interlayer coupling based on Eq. (5) for (001), (110), and (111) orientations and the results are summarized in Table II. I_0 in the table is obtained by using the group velocities and curvature radii inferred from the experimental Cu Fermi surface in Ref. 27. We can also calculate I_0 from the TB model and those values are a little larger than those shown in the table mainly due to the larger group velocity. I_0 is

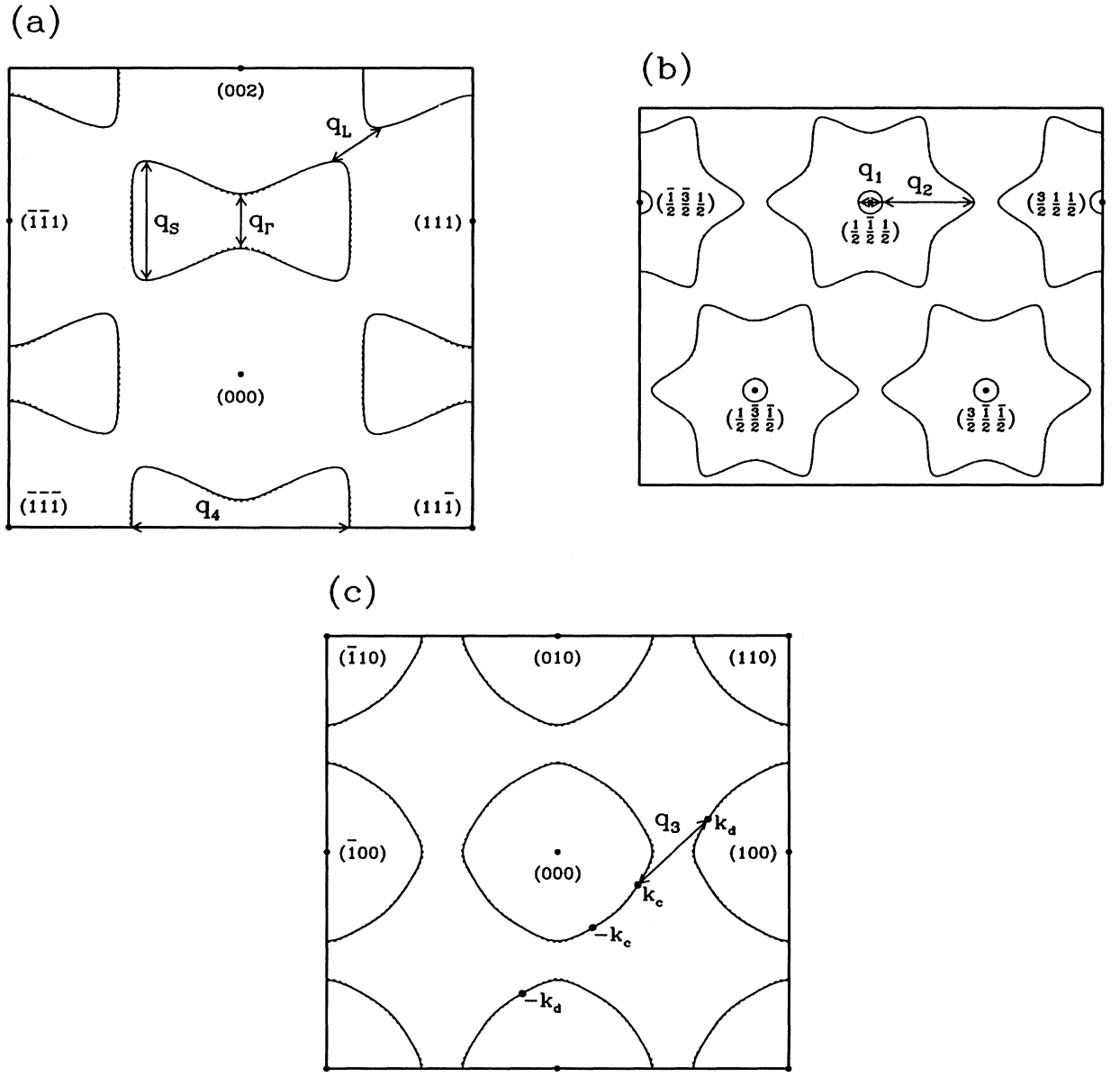

FIG. 1. Cross sections of the Cu Fermi surface. Solid curves are from our calculation and the dotted curves are from the de Haas–van Alphen data (Ref. 27). (a) The cross-sectional plane contains the $k_x = k_y$ and k_z axes. (b) The cross-sectional plane contains the center of the neck $[(\frac{1}{2}\frac{\bar{1}}{2}\frac{1}{2})]$ and is perpendicular to the $[1\bar{1}1]$ direction. Small circles are cross sections of necks. (c) The cross-sectional plane contains the k_x and k_y axes. $\pm k_c$ and $\pm k_d$ indicate the intersection of the Fermi surface with a line that contains the spanning vector q_3. Experimental spanning vectors are indicated by arrows. q_Γ and q_S in (a) are for the (001) orientation. q_L in (a) is for the (111) orientation. q_1 and q_2 in (b), q_3 in (c), and q_4 in (a) are for the (110) orientation.

TABLE I. On-site energies of Co for each spin. The unit is Ry.

	E_s	E_p	$E_{d_{xy}}$	$E_{d_{x^2-y^2}}$
Majority	1.158 46	1.760 62	0.556 67	0.560 70
Minority	1.177 46	1.770 62	0.672 97	0.676 45

just the "geometrical weight" used in Ref. 12, but the values in Ref. 12 are obtained from their calculated band structures which can be off by as much as a factor of 3 compared to values obtained from the actual Fermi-surface data. It is shown that the spin asymmetry of the reflection amplitude varies at each extremal point and is

TABLE II. Strength of the interlayer coupling in fcc Co/Cu/Co. I_0 is determined from the experimental Cu Fermi surface (Ref. 27). The thickness of the spacer layer is taken as $D = 10$ Å.

Orientation	q_{ij}^{α}	Period (Å)	I_0 (mRy)	$\lvert\Delta r\rvert$	$I_0\lvert\Delta r\rvert^2/D^2$ (mJ/m^2)
(001)	q_Γ	10.6	5.0	0.044	0.021
	q_S	4.6	11	0.53	6.7
(110)	q_1	12.2	2.6	0.43	1.0
	q_2	3.2	7.3	0.015	0.0036
	q_3	4.2	0.80	0.13	0.030
	q_4	2.7	88	0.45	38
(111)	q_L	9.4	1.3	0.46	0.59

the crucial factor which determines the coupling strength for each period. We shall discuss our analyses for (001), (110), and (111) orientations separately.

A. (001) orientation

For the (001) orientation, there are two nonequivalent extremal spanning vectors q_Γ and q_S as shown in Fig. 1(a). Their corresponding $\mathbf{k}_{\|}$'s are denoted by $\mathbf{k}_\Gamma$ and $\mathbf{k}_S$. $\mathbf{k}_\Gamma = 0$ and q_Γ leads to a longer period of 10.6 Å. $\mathbf{k}_S = (0.41, 0.41, 0)\frac{2\pi}{a}$ and q_S leads to a shorter period of 4.6 Å. As shown in Table II, the coupling strengths of q_Γ and q_S are totally different due to the difference in $|\Delta r|$. This is easily illustrated with the bulk band structures for $\mathbf{k}_{\|} = \mathbf{k}_\Gamma$ [Fig. 2(a)] and $\mathbf{k}_{\|} = \mathbf{k}_S$ [Fig. 2(b)]. For both cases, Cu and Co with majority spin have a predominantly *sp*-like band at the Fermi level and $|r^+|$ is small. However, Co with minority spin has completely different band structures for $\mathbf{k}_{\|} = \mathbf{k}_\Gamma$ and $\mathbf{k}_{\|} = \mathbf{k}_S$ at the Fermi level. For $\mathbf{k}_{\|} = \mathbf{k}_\Gamma$, there are two states in Co (with different k_z's) having the same (Δ_1) symmetry as the incoming wave, thus significant transmission occurs and $|r^-|$ is small. On the other hand, for $\mathbf{k}_{\|} = \mathbf{k}_S$, the available state in Co has a different symmetry [see Fig. 2(b)] and total reflection occurs ($|r^-| = 1$). In Fig. 2(b), we label states which are symmetric (antisymmteric) with respect to the exchange of x and y coordinates by A_1 (A_2), since the space group for this case has only two one-dimensional irreducible representations. As a result, $|\Delta r|$ is small for $\mathbf{k}_{\|} = \mathbf{k}_\Gamma$ and large for $\mathbf{k}_{\|} = \mathbf{k}_S$ at the Fermi level. For $\mathbf{k}_{\|} = \mathbf{k}_S$, $|\Delta r|$ is slightly bigger than 0.5 because of the phase difference between r^+ and r^-. The situation for $\mathbf{k}_{\|} = \mathbf{k}_S$ is similar to the complete quantum-confinement model[4] and yields a strong coupling.

In Fig. 3, $|r^+|$ (solid) and $|r^-|$ (dotted) are plotted as a function of energy for $\mathbf{k}_{\|} = \mathbf{k}_\Gamma$ and $\mathbf{k}_{\|} = \mathbf{k}_S$ around the Fermi level. For both cases, $|r^+|$ is small. For $\mathbf{k}_{\|} = \mathbf{k}_S$, total reflection occurs abruptly near -1 eV ($|r^+|$=1) due to the existence of a tiny gap between the two A_1 bands caused by anticrossing [too small to be seen clearly in the middle panel of Fig. 2(b)]. When a gap occurs between two A_1 bands in Co, the incident wave of A_1 symmetry

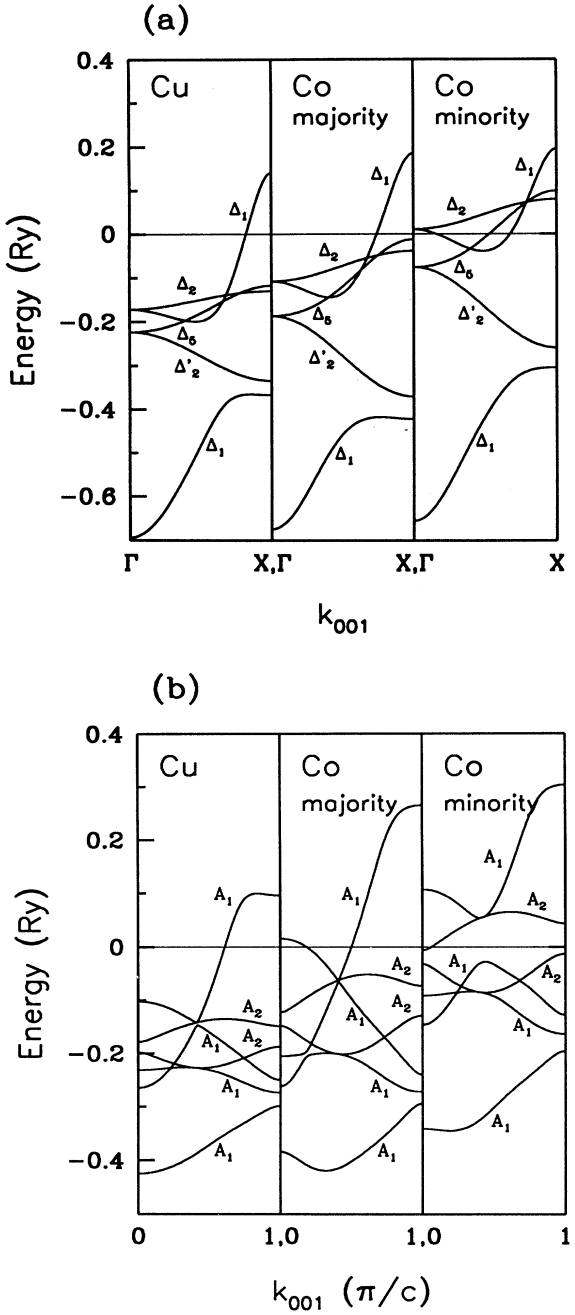

FIG. 2. Bulk band structures of fcc Cu and Co for the (001) orientation for (a) $\mathbf{k}_{\|} = 0$ and (b) $\mathbf{k}_{\|} = \mathbf{k}_S = (0.41, 0.41, 0)\frac{2\pi}{a}$. Here $c = \frac{a}{2}$.

with energy inside the gap is totally reflected. Near the Fermi level, most of the differences in reflection amplitudes come from the minority-spin bands. For $\mathbf{k}_{\|} = \mathbf{k}_\Gamma$, $|r^-|$ is small very near the Fermi level and increases rapidly below the Fermi level as the group velocity of minority spin Co bands decreases. $|r^-|$ finally becomes one when the group velocity is zero at the bottom of the Δ_1 band. Below that point ($E \sim -0.55$ eV), total reflec-

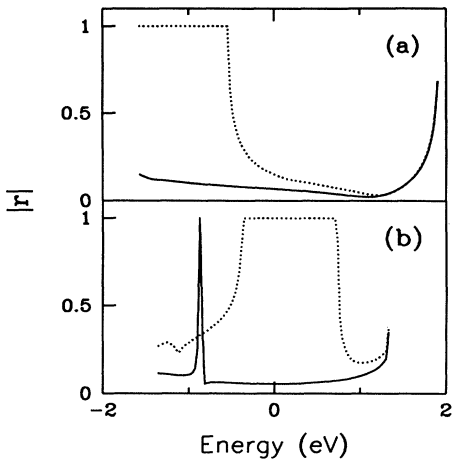

FIG. 3. Reflection amplitudes as a function of energy for the majority (solid curve) and the minority (dotted) spin for the (001) orientation for (a) $\mathbf{k}_{\|} = 0$ and (b) $\mathbf{k}_{\|} = \mathbf{k}_S$.

tion occurs due to the absence of available states with the same symmetry. For $\mathbf{k}_{\|} = \mathbf{k}_S$, $|r^-| = 1$ at the Fermi level due to the symmetry mismatch. Away from the Fermi level, an incoming wave is partially transmitted as the bands with A_1 symmetry become available in Co. The recent spin-dependent photoemission experiment[29] shows that electrons with minority spin are more strongly confined for $\mathbf{k}_{\|} = 0$, which qualitatively agrees with our result [see Fig. 3(a)]. However, unlike the Fe magnetic layer, the complete confinement of electrons with the minority spin and $\mathbf{k}_{\|} = 0$ in the spacer is not expected at the Fermi level.

Nordström *et al.*[19] calculated the interlayer coupling for (001) Co/Cu/Co sandwiches with 5-, 7-, and 11-ML magnetic layers, using a Green's-function method. The coupling for each period is obtained by partitioning the $\mathbf{k}_{\|}$ domain. They found that the coupling of the short period is almost the same for 5-, 7-, and 11-ML Co layers. A coupling strength of about 4 mJ/m^2 at 10 Å for the short-period oscillation is inferred from their result, which agrees well with our result of 6.7 mJ/m^2. On the other hand, the strength for the long-period coupling varies with the thickness of the magnetic layer and the coupling strength for the 5- and 7-ML case is much bigger than our result. However, for the 11-ML case, the coupling strength decreased noticeably and became almost invisible for thicker spacers. Note that our result corresponds to the case of infinite Co layer thickness. Kudrnovský *et al.*[20] evaluated interlayer coupling of the long and short periods for the 1-ML and semi-infinite Co layers. They found that the long-period coupling is suppressed for the semi-infinite Co layer and the coupling strength for the short period is about 8.7 mJ/m^2, which agrees well with our result. The change of electronic structure in very thin Co layers and how it changes reflection amplitudes in the Cu spacer need to be studied further in detail.

There are several experimental results available for samples grown by molecular-beam epitaxy (MBE) along the [001] direction. Johnson *et al.*[5] measured the exchange coupling of Co/Cu/Co sandwiches as a function of Cu layer thickness with Co layer thickness fixed at 60 Å (about 35 ML). The measured coupling strength was about 0.4 mJ/m^2 at ~6.6 Cu ML. Five antiferromagnetic peaks were observed and their positions agree well with the short-period oscillation predicted by the theoretical calculations of Nordström *et al.*,[19] except that the theoretically predicted peak at 9 ML was missing in the experimental observation. Since there is a strong ferromagnetic peak (at 8 ML) preceding this antiferromagnetic peak (see Fig. 2 of Ref. 19), the effect of interface roughness may average out these two peaks and cause the antiferromagnetic peak to be absent. Since the averaging of the ferromagnetic and antiferromagnetic coupling may depend on the degree of interface roughness, we expect the coupling strength to be sample dependent. Indeed, this missing peak was observed by Bloeman *et al.*[30] with a ferromagnetic bias. The observed coupling strength is smaller than the theoretical predictions, which is expected, considering the effects of the interface roughness and finite temperature. Since only a few peaks were observed, it is difficult to obtain two periods in a reliable way by fitting the data. This point is further illuminated by comparing with other experiments. Qiu, Pearson, and Bader[31] reported the observation of three antiferromagnetic peaks with a period of ~5.5 ML with a number of MBE grown Co/Cu/Co samples. Different Co layer thickness with 8, 14, and 20 ML were studied and the results appear to be independent of the magnetic-layer thickness. At first sight, it can be argued that the short period is wiped out due to the interface roughness and only the long period survives. However, the positions of the observed peaks in Ref. 31 are almost out of phase with the long-period antiferromagnetic peaks predicted by the theoretical studies.[19] Instead they agree well with the theoretically predicted short-period peaks, if we assume that the theoretical peaks at 9 and 14.5 ML were averaged out with neighboring ferromagnetic peaks by interface roughness. The coupling strength of this observation was 0.08 mJ/m^2 at 6.2 ML,[32] which is much smaller than the theoretical value for the short-period oscillation (perhaps due to a strong smearing effect of the interface roughness), but about four times bigger than our theoretical value for the long-period oscillation. Therefore, we suspect that the peaks observed in Ref. 31 are superpositions of long-period and short-period oscillations (including the smearing effect), while the short-period coupling plays a more important role.

B. (110) orientation

For the (110) orientation there are four possible periods, associated with three different $\mathbf{k}_{\|}$'s: $\mathbf{k}_1$, $\mathbf{k}_2$, and $\mathbf{k}_3$. $\mathbf{k}_1 = (\frac{1}{2}, -\frac{1}{2}, \frac{1}{2})\frac{2\pi}{a}$ is at the center of the neck of the Cu Fermi surface and it is associated with two different extremal spanning vectors q_1 and q_2 [Fig. 1(b)]. They lead to the periods 12.3 and 3.2 Å, respectively. $\mathbf{k}_2 = (\frac{1}{4}, -\frac{1}{4}, 0)\frac{2\pi}{a}$ with the spanning vector q_3 which passes through the X point (projected in the plane) as

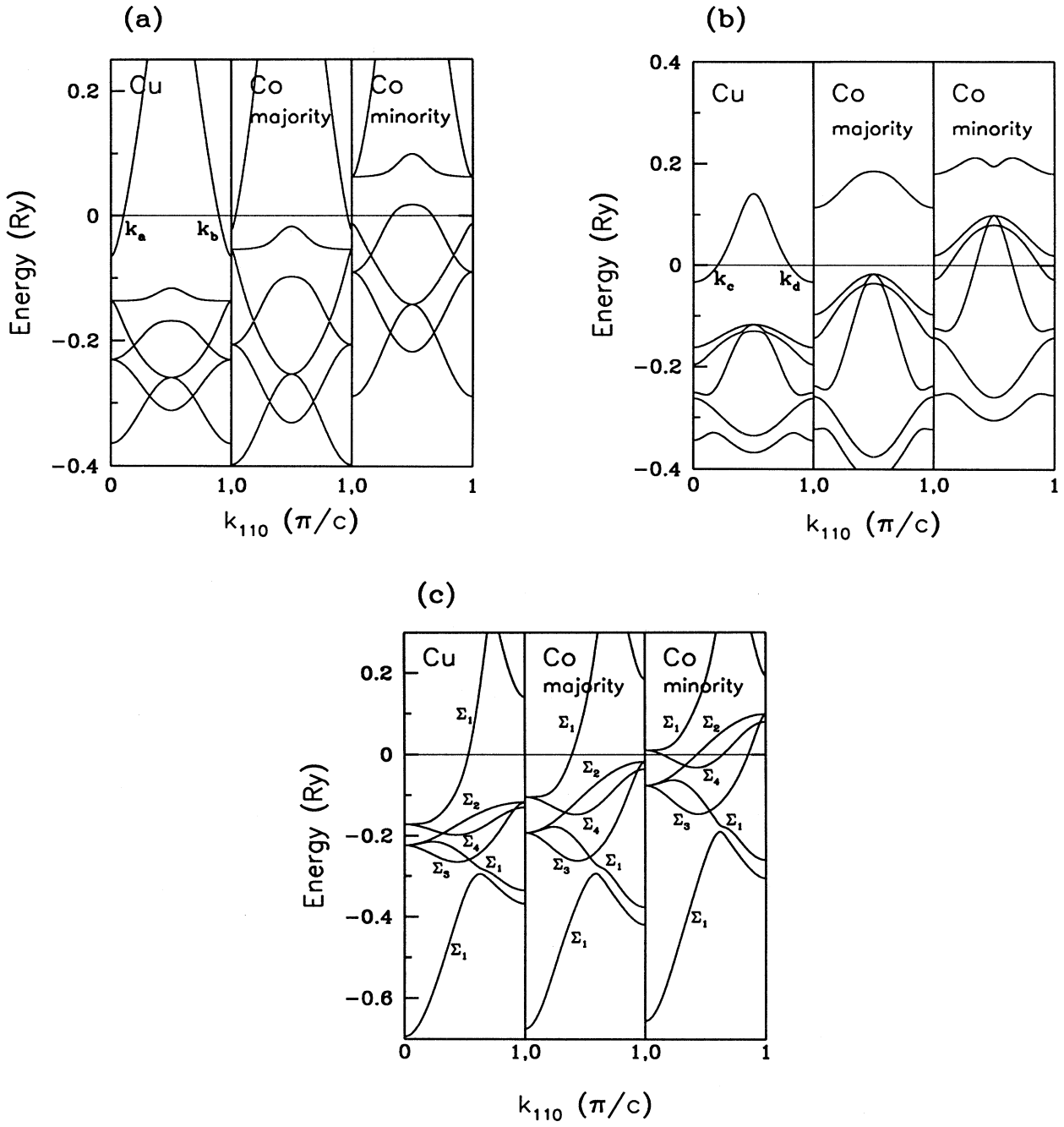

FIG. 4. Bulk band structures of Cu and Co for the (110) orientation for (a) $\mathbf{k}_{\|} = \mathbf{k}_1 = (\frac{1}{2}, -\frac{1}{2}, \frac{1}{2})\frac{2\pi}{a}$, (b) $\mathbf{k}_{\|} = \mathbf{k}_2 = (\frac{1}{4}, -\frac{1}{4}, 0)\frac{2\pi}{a}$, and (c) $\mathbf{k}_{\|} = \mathbf{k}_3 = 0$. Here $c = \frac{a}{2\sqrt{2}}$.

shown in Fig. 1(c). q_3 gives rise to the 4.19 Å period. $\mathbf{k}_3 = 0$ with the spanning vector q_4 shown in Fig. 1(a), which gives rise to a period of 2.7 Å.

Bulk energy bands for $\mathbf{k}_{\|} = \mathbf{k}_1$ are shown in Fig. 4(a). In Cu, there is a band gap and lower bands are completely immersed below the Fermi level. These completely filled bands make little contribution to the interlayer coupling. Cu has four k_z vectors at the Fermi level, which are denoted by $\pm k_a$ and $\pm k_b$. Each of the two nonequivalent spanning vectors q_1 and q_2 is related to two possible combinations of $\pm k_a$ and $\pm k_b$. $k_a \to -k_a$ and $-k_b \to k_b$ lead to q_1, while $k_a \to k_b$ and $-k_b \to -k_a$ lead to q_2. For the incoming wave with $k_z = k_a$, there are two reflected waves with $k_z = -k_a$ and k_b. We define each reflection amplitude as $r_{aa} = r(k_a \to -k_a)$ and $r_{ab} = r(k_a \to k_b)$. Similarly, $r_{bb} = r(-k_b \to k_b)$ and $r_{ba} = r(-k_b \to k_a)$.

In Co with majority spin, the states near the Fermi level have the same character (predominantly *sp*-like) as the incident waves and both $|r^+_{aa}|$ and $|r^+_{ab}|$ are small. For the minority-spin electron, the incoming wave is almost totally reflected, since the states available in Co now have very different character (predominantly *d*-like). However, the incoming wave is mostly reflected to $-k_a$ rather than k_b although they have the same symmetry. This seems to be related to the larger overlap between two wave functions with k_a and $-k_a$ than between those with k_a and k_b. This property can be explained only when hybridized wave functions are examined. It is found that $|\Delta r_{aa}| = |\Delta r_{bb}| = 0.43$ and $|\Delta r_{ab}| = |\Delta r_{ba}| = 0.015$. As a result, the shorter period is not detectable although it has a bigger geometrical weight. In Ref. 19, these two periods could not be separated by partitioning the $\mathbf{k}_\parallel$ domain because they corresponds to the same $\mathbf{k}_\parallel$. Our result clearly explains why the shorter period is not visible. The coupling strength of the longer period obtained in Ref. 19 is in good agreement with ours.

Figure 4(b) shows the band structure for $\mathbf{k}_\parallel = \mathbf{k}_2$. There are also four k_z values (denoted by $\pm k_c$ and $\pm k_d$) in Cu at the Fermi level. Here $k_c \rightarrow k_d$ and $-k_d \rightarrow -k_c$ correspond to the same spanning vector q_3 which lead to a period of 4.19 Å. Note that $k_c \rightarrow -k_c$ or $-k_d \rightarrow k_d$ does not lead to an extremal spanning vector, which can be seen in Fig. 1(c). Since the Fermi level falls within the band gap in Co with the majority spin, the incoming wave is totally reflected for the majority spin. For the minority spin the incident wave is partially reflected, since a state with the same symmetry can be found in Co. This is in contrast with other extremal points where total reflection occurs for minority spin instead of majority spin, and it shows that degree of confinement of electrons with each spin depends on the detailed band structure at each extremal point. For the incoming wave with $k_z = k_c$ $(-k_d)$, there are two reflected waves with $k_z = k_d$ or $-k_c$ and the reflection amplitude for state k_d $(-k_c)$ is small. Thus, the interlayer coupling for this period is very weak, which agrees with other theoretical studies.[19]

Energy bands for $\mathbf{k}_\parallel = \mathbf{k}_3 = 0$ are shown in Fig. 4(c). Total reflection occurs for minority spin due to the mismatch in band symmetry whereas large transmission occurs for majority spin, since a state with character similar to the incident wave is found in Co. The large $|\Delta r|$ combined with the large geometrical weight of the Cu Fermi surface leads to very strong coupling (38 mJ/m^2) for $\mathbf{k}_\parallel = \mathbf{k}_3$. However, because the period is very short (about 2 ML or 2.7 Å), it is not likely to be observed experimentally. Due to the lattice mismatch between Cu and Co, it would be difficult to get sharp interfaces. Two points are worth mentioning here. First, considerable strain is expected in the Co layer when it is grown on Cu substrate due to the 4% lattice mismatch. In Co with minority spin, the band with character similar to the incident wave from Cu is just above the Fermi level [see Fig. 4(c)]. This band might be lowered slightly below the Fermi level due to the sample condition such as the strain effect. Thus, a very small change of band structure can cause a big difference in $|\Delta r|$ and thus the coupling strength at this extremal point. Second, when the curvature radius of the Fermi surface is large, the asymptotic equation given in Eq. (3) is a good approximation only for a relatively thicker spacer layer. When the Fermi surface is truly nested as in (001) Cr (which is believed to be responsible for the short period for that orientation), the interlayer coupling should be obtained by an integration over the nested region as done in Ref. 33.

For MBE grown samples grown along the [110] direction, only the long-period oscillation was observed.[6] This seems reasonable since the other possible periods are either too short (about 2 ML) or too weak to be observed. The observed peak positions are consistent with the theoretical calculation reported in Ref. 19. The measured coupling strength is about 0.7 mJ/m^2 at 8.5 Å, which is consistent with our result (1 mJ/m^2 at 10 Å).

C. (111) orientation

Currently, there is a difficulty in growing good quality samples by MBE along the [111] direction.[34,35] On the other hand, the (111) magnetic multilayers can provide a critical test for the theory, since there is only one nonequivalent extremal spanning vector for this orientation and the period is long so that the coupling strength will be relatively less affected by the interface roughness. As shown in Fig. 1(a), the extremal spanning vector q_L passes through the center of the neck of the Cu Fermi surface for this orientation and the corresponding $\mathbf{k}_\parallel$ is $\mathbf{k}_L = (\frac{1}{3}, \frac{1}{3}, -\frac{2}{3})\frac{2\pi}{a}$. Bulk band structures for the (111) orientation for $\mathbf{k}_\parallel = \mathbf{k}_L$ are shown for $-\pi/c < k_z < \pi/c$ ($k_z = k_{[111]}$) in Fig. 5, where the spacing between two adjacent planes is $c = a/\sqrt{3}$. Note that the band structure has a reflection symmetry about the axis at some finite k_z, instead of $k_z = 0$ [reflection axis for (001) and (110) orientations]. Since the band in Co with majority spin has similar character to that in Cu at the Fermi level, large transmission is expected. For the minority spin,

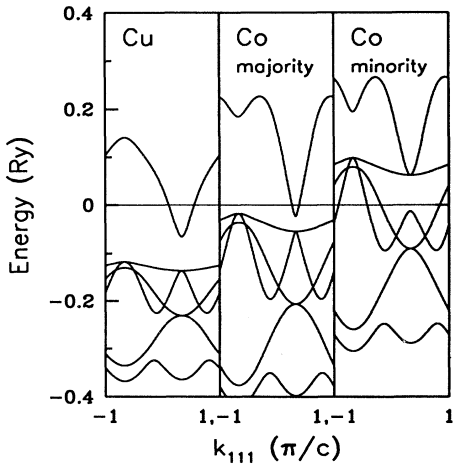

FIG. 5. Bulk band structures of Cu and Co for the (111) orientation for $\mathbf{k}_\parallel = \mathbf{k}_L = (\frac{1}{3}, \frac{1}{3}, -\frac{2}{3})\frac{2\pi}{a}$. Here $c = \frac{a}{\sqrt{3}}$.

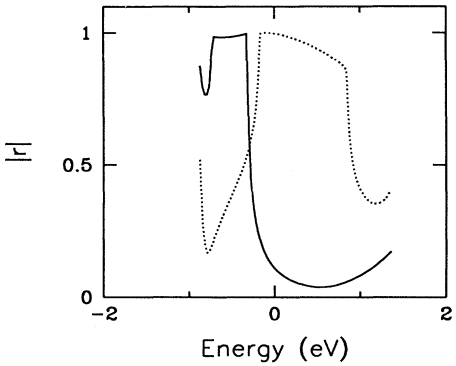

FIG. 6. Reflection amplitudes as a function of energy for the majority (solid curve) and the minority (dotted) spin for $\mathbf{k}_{\|} = \mathbf{k}_L$ for the (111) orientation.

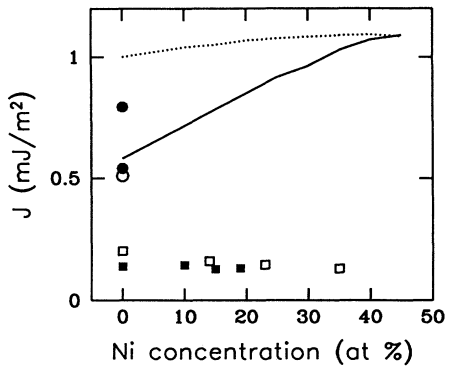

FIG. 7. Estimated coupling strength in $Co/Cu_{1-x}Ni_x/Co$ as a function of Ni concentration for the (111) (solid curve) and (110) (dotted curve) orientation at $D = 10$ Å. The circles are experimental results for Co/Cu/Co with MBE grown samples (Refs. 6 and 36) for the (111) (solid) and (110) (open) orientations. The squares are from the sputtered samples for the (111) (solid) (Ref. 9) and (110) (open) (Ref. 7) orientation. Experimental coupling strength are from the first antiferromagnetic peak and scaled to $D = 10$ Å.

there are two waves with positive group velocities at the Fermi level. One has the "wrong" symmetry and does not couple with the incident wave. The other has the "right" symmetry, but different character [i.e., the overlap of the state with the incident wave is small (~ 0.1)]. Thus, transmission is weak and $|r^-|$ is almost one. The magnitude of the reflection amplitude of each spin for energies around the Fermi level is displayed in Fig. 6. Near the Fermi level, the electrons with the minority spin are highly confined and $|r^-|$ decreases sharply for energies below the Fermi level as new states with character similar to the incident wave appear. Here, we find that besides band symmetry, the detailed character of the state also plays an important role in determining $|\Delta r|$ and the coupling strength.

All available experimental observations for this orientation are in good agreement with our result. In the samples grown by MBE, the coupling strength was found to 1.1 mJ/m^2 at 8.5 Å (Ref. 6) and 0.54 mJ/m^2 at 10 Å (Ref. 36) (to be compared with our result of 0.59 mJ/m^2 at 10 Å). In sputtered samples, the coupling strength is weaker but of the same order of magnitude.[37,38]

IV. fcc $Co/Cu_{1-x}Ni_x/Co$ SANDWICHES

In this section, we examine the exchange coupling of magnetic multilayers made of Co and $Cu_{1-x}Ni_x$ within the virtual crystal approximation. TB parameters for paramagnetic Ni are taken from Ref. 26 and the linear interpolation scheme is used[8] for the TB parameters of $Cu_{1-x}Ni_x$. Scattering due to alloy disorder is neglected in our calculation. The change of period was already given in earlier studies[8,9] and we focus on the change of coupling strength for the (111) and (110) orientations in this paper. For the (110) orientation, the short period is assumed to be completely wiped out due to the interface roughness. Then, only one long period for each orientation needs to be considered, which is related to the neck of the Cu Fermi surface. In Fig. 7, the coupling strength in $Co/Cu_{1-x}Ni_x/Co$ is plotted as a function of the Ni concentration for the (111) (solid curve) and (110) (dotted) orientation. The group velocity and the curvature radius of the Fermi surface in $Cu_{1-x}Ni_x$ at the extremal point is calculated from the TB model since experimental values are not available. For Cu ($x = 0$), our calculated values are off by 17 and 28 % in the geometrical weight I_0 for the (111) and (110) orientations, respectively. Note that in the previous section I_0 is obtained based on the experimental data for the Fermi surface. Most of the error comes from the group velocity. To compensate for this error, the theoretical curves in Fig. 7 are scaled down such that the coupling in Co/Cu/Co is the same as that obtained in the previous section.

The coupling strength increases as a function of Ni concentration for the (111) orientation. This is mainly due to the change of the geometrical weight I_0. Both the average group velocity and the average curvature radius of the $Cu_{1-x}Ni_x$ Fermi surface increase with similar rate. $|r^+|$ and $|r^-|$ remain almost unchanged. For the (110) orientation, the increase of the coupling strength is very small. As Ni concentration increases, the group velocity slightly decreases and the curvature radius of the $Cu_{1-x}Ni_x$ Fermi surface slightly increases. As a result, I_0 remains unchanged as a function of x. However, $|\Delta r|$ increases gradually since $|r^+|$ decreases as a function of x while $|r^-| \approx 1$ for all x.

Our results are compared with available experimental data. The first antiferromagnetic peaks are taken from the data and their strengths are scaled to give coupling strengths at $D = 10$ Å. Circles are from MBE grown Co/Cu/Co samples[6,36] for the (111) (solid) and (110) (open) orientation. Squares are from sputtered $Co/Cu_{1-x}Ni_x/Co$ multilayers. The coupling strength is much weaker for the sputtered samples. For the (111) orientation (solid square),[9] the strengths are almost same for $x = 0, 10, 15$, and 19 %. For the (110) direction (open square)[7,32] the coupling strength decreases slightly as the

Ni concentration increases. These trends do not compare favorably with our results.[39] This discrepancy implies that the coupling strength in $Co/Cu_{1-x}Ni_x/Co$ may be affected considerably by disorder and defects in the sputtered samples. In an earlier study,[40] the coupling strength of the alloy spacer is predicted to decay exponentially as a function of x in the dilute limit. It is attributed to the finite lifetime of the quasiparticle due to the incoherent scattering.

V. CONCLUSION

We have presented a method to calculate the reflection amplitudes within the TB scheme and estimated the coupling strength in Co/Cu/Co multilayers for all possible periods for (001), (110), and (111) orientations by using the spin asymmetry of the reflection amplitude, Δr. The estimated coupling strengths are consistent with other first-principles calculations and in good agreement with experimental observations for (110) and (111) orientations. For the (001) orientation, the strength of the shorter-period coupling seems to be weakened considerably by the interface roughness and we could not extract reliable strength for the longer period from the experiment. $|\Delta r|$ varies from one extremal point to another and is the crucial factor for determining the coupling strength. We have shown that among possible periods predicted from the spacer Fermi surface some have too small coupling strengths to be observed experimentally due to the small $|\Delta r|$. When the incident wave is well transmitted for one spin component and totally reflected for another, strong coupling strength is obtained. This is analogous to the complete quantum-confinement model. The presence of a band gap or mismatch of band symmetry for incident and transmitted waves is not the only reason for the large reflection amplitude. More detailed properties such as overlap between incident and transmitted states should be considered. Realistic band structures including *sp-d* hybridization are needed for this purpose. When the incident wave is reflected into more than one wave, the reflection amplitude can be totally different for each reflected wave with the same symmetry. This case is clearly shown in (110) Co/Cu/Co. The reflection amplitude also depends on the properties of two wave functions in the spacer corresponding to a given period and when these two states do not couple well, the interlayer coupling is very weak. For the transition-metal spacer, this mechanism is expected to play an important role since there are many bands near the Fermi level. We have also calculated the change of the coupling strength in $Co/Cu_{1-x}Ni_x/Co$ system. Our results do not agree with experimental data from the sputtered samples and this discrepancy may be partly due to the incoherent electron scattering by disorder and defects.

ACKNOWLEDGMENTS

This work is supported by the University of Illinois research board and the University of Illinois Materials Research Laboratory through Contract No. NSF/DMR-89-20538.

APPENDIX A: DERIVATION OF THE INTERLAYER COUPLING

Combining Eqs. (1) and (2) in Sec. II, we have

$$J = -\frac{1}{8\pi^3}\mathrm{Im}\int d^2\mathbf{k}_{\parallel}\int_{-\infty}^{+\infty} d\varepsilon f(\varepsilon)\sum_{n=1}^{\infty}\frac{1}{n}\,\mathrm{Tr}\,[(G_0T^{L,\mathrm{F}}G_0T^{R,\mathrm{F}})^n-(G_0T^{L,\mathrm{AF}}G_0T^{R,\mathrm{AF}})^n], \tag{A1}$$

where $\mathrm{Tr}=\frac{c}{2\pi}\sum_\sigma\int dk_z$, which denotes the trace over all Bloch states for the spacer material with σ being the spin index ($\uparrow$ or $\downarrow$) and c is the distance between two adjacent atomic planes. The magnetic moment of the left magnetic layer (L) is fixed to be upward. Then, the magnetic moment of the right magnetic layer (R) is parallel or antiparallel to that of L depending on the coupling configuration. Suppose that there are N real wave vectors (denoted by k_i^+) for waves propagating to the right with energy ε. There are also N real wave vectors (denoted by k_i^-) for waves traveling to the left.

Carrying out the integral over k_z for terms in the trace of Eq. (A1) via the contour-integral method, we obtain (with ν =F or AF denoting the ferromagnetic or antiferromagnetic configuration)

$$\left(\frac{c}{2\pi}\right)^2\int dk_z\int dk_z'\langle k_z\sigma|G_0|k_z\sigma\rangle\langle k_z\sigma|T^{L,\nu}|k_z'\sigma\rangle\langle k_z'\sigma|G_0|k_z'\sigma\rangle\langle k_z'\sigma|T^{R,\nu}|k_z\sigma\rangle=\sum_{ij}\mathcal{R}_{ij}^{L,\nu,\sigma}\mathcal{R}_{ji}^{R,\nu,\sigma}, \tag{A2}$$

where $\mathcal{R}^{L,\nu,\sigma}$ and $\mathcal{R}^{R,\nu,\sigma}$ are $N\times N$ matrices with

$$\begin{aligned}\mathcal{R}_{ij}^{L,\nu,\sigma}&=e^{ik_j^-z_L}\,r_{ji}^{L,\nu,\sigma}\,e^{-ik_i^+z_L},\\ \mathcal{R}_{ij}^{R,\nu,\sigma}&=e^{ik_j^+z_R}\,r_{ji}^{R,\nu,\sigma}\,e^{-ik_i^-z_R}.\end{aligned} \tag{A3}$$

$r_{ji}^{L,\nu,\sigma}$ and $r_{ji}^{R,\nu,\sigma}$ are reflection amplitudes,

$$\begin{aligned}r_{ji}^{L,\nu,\sigma}&=r^{L,\nu,\sigma}(k_j^-\to k_i^+),\\ r_{ji}^{R,\nu,\sigma}&=r^{R,\nu,\sigma}(k_j^+\to k_i^-),\end{aligned} \tag{A4}$$

and z_L (left) and z_R (right) are positions of the two interfaces. The thickness of the spacer is $D = |z_L - z_R|$. While the up-spin ($\uparrow$) is always the majority spin in layer L, it can be the majority or minority spin in layer R depending on whether the configuration is ferromagnetic (F) or antiferromagnetic (AF). Thus we have

$$r_{ij}^{L,+} = r_{ij}^{L,\mathrm{F},\uparrow} = r_{ij}^{L,\mathrm{AF},\uparrow}$$
$$r_{ij}^{R,+} = r_{ij}^{R,\mathrm{F},\uparrow} = r_{ij}^{R,\mathrm{AF},\downarrow}. \tag{A5}$$

The trace can be written as $\sum_{\mu=1}^{2N}[(\lambda_\mu^{\mathrm{F}})^n - (\lambda_\mu^{\mathrm{AF}})^n]$, where λ_μ^{F} and $\lambda_\mu^{\mathrm{AF}}$ are the eigenvalues of $2N \times 2N$ matrices $\mathcal{R}^{\mathrm{F}}$ and $\mathcal{R}^{\mathrm{AF}}$ with

$$\mathcal{R}^{\nu} = \begin{pmatrix} \mathcal{R}^{L,\nu,\uparrow}\mathcal{R}^{R,\nu,\uparrow} & 0 \\ 0 & \mathcal{R}^{L,\nu,\downarrow}\mathcal{R}^{R,\nu,\downarrow} \end{pmatrix}. \tag{A6}$$

When the spacer is thick, the integration over ε and $\mathbf{k}_\parallel$ can be performed by using the contour integral and stationary phase approximation. When it is expanded as a power series of n, the coefficients can be shown to decay as $1/n^3$. Therefore, the interlayer coupling is dominated by the leading term.[18] Keeping only the leading term, we have

$$\sum_{\mu=1}^{2N}(\lambda_\mu^{\mathrm{F}} - \lambda_\mu^{\mathrm{AF}}) = 4\sum_{i,j=1}^{N}\Delta r_{ij}^{L}\Delta r_{ji}^{R}e^{iq_{ij}D}, \tag{A7}$$

where Δr is the spin asymmetry of the reflection amplitudes. When the two magnetic layers are made of the same material (Co in this case), $\Delta r_{ij} \equiv \Delta r_{ij}^{R} = \Delta r_{ji}^{L}$ and J is given in Eq. (3) of Sec. II.

APPENDIX B: CALCULATION OF THE REFLECTION AMPLITUDE

We calculate the reflection amplitudes using the empirical TB method with two center integrals.[41] Let N_B be the number of basis orbitals. In this paper, s, p^3, and d^5 orbitals are included and $N_B = 9$. A planar orbital state is denoted by $|\mathbf{k}_\parallel, l; \alpha\rangle$, where l designates the atomic-plane position and α labels the nine atomic orbitals. In the planar orbital basis, $H^{(\sigma)}(\mathbf{k}_\parallel)$ represents a matrix which couples a given atomic plane to the σth neighboring plane. The matrix element is given by

$$H_{\alpha,\alpha'}^{(\sigma)}(\mathbf{k}_\parallel) = \langle \mathbf{k}_\parallel, l; \alpha|(H - E)|\mathbf{k}_\parallel, l + \sigma; \alpha'\rangle, \tag{B1}$$

where H is the Hamiltonian and E is the energy. The matrix elements of $H-E$ defined in the three-dimensional TB basis ($|\mathbf{k}, \alpha\rangle$) can be written as polynomials in $e^{ik_z c}$ with $H^{(\sigma)}$ as the coefficients,

$$\langle \mathbf{k}, \alpha|H - E|\mathbf{k}, \alpha'\rangle = \sum_{\sigma=-m}^{m} H_{\alpha,\alpha'}^{(\sigma)}(\mathbf{k}_\parallel)e^{i\sigma k_z c}. \tag{B2}$$

c is the distance between two adjacent atomic planes, k_z is the wave vector perpendicular to the plane, and m is the number of neighboring planes coupled to the center plane on each side. In this paper, interactions up to the second-nearest neighbor are included. For the fcc crystal we have $m = 2$ for the (001) or (110) orientation and $m = 1$ for the (111) orientation. From now on, we consider the $m = 2$ case for convenience. It can be easily extended to the general case. In order to calculate reflection amplitudes, all bulk solutions including the evanescent states (complex k_z) are needed. They can be obtained from the "companion matrix"[25]

$$\begin{pmatrix} 0 & 1 & 0 & 0 \\ 0 & 0 & 1 & 0 \\ 0 & 0 & 0 & 1 \\ -H^{(+2)^{-1}}H^{(-2)} & -H^{(+2)^{-1}}H^{(-1)} & -H^{(+2)^{-1}}H^{(0)} & -H^{(+2)^{-1}}H^{(+1)} \end{pmatrix}, \tag{B3}$$

where 1 is the identity matrix of the same dimension as H. The eigenvalues of the above matrix are $e^{ik_z c}$ with k_z in general a complex number. The eigenvector associated with $k_z = k_j$ is denoted by C_j with its ith component denoted by $C_{j,i}$ ($i = 1, ..., 2mN_B$). In general, the number of solutions is $N_A = 2mN_B$. Note that $C_{j,mN_B+\alpha}$ ($\alpha = 1, 2, \cdots, N_B$) represents the projection of the jth state onto the basis orbital α at the zeroth atomic plane.

We consider a heterostructure which consists of materials I (with $l = -1, -2, -3, \ldots$) and II (with $l = 0, 1, 2, 3, \ldots$). For an incoming wave (from the left) with $k_z = k_i^I$ in material I, reflection occurs at the interface (midway between $l = -1$ and $l = 0$). We express the wave function as a linear combination of bulk propagating and evanescent states.

$$|\psi_i\rangle = \sum_{l=-\infty}^{-1} e^{ik_i^I(l+1/2)c}\sum_{\alpha=1}^{N_B} C_{i,mN_B+\alpha}^{I}|\mathbf{k}_\parallel, l; \alpha, I\rangle + \sum_{j=1}^{N_A/2} r_{ij}\sum_{l=-\infty}^{-1} e^{ik_j^I(l+1/2)c}\sum_{\alpha=1}^{N_B} C_{j,mN_B+\alpha}^{I}|\mathbf{k}_\parallel, l; \alpha, I\rangle$$
$$+ \sum_{j=1}^{N_A/2} t_{ij}\sum_{l=0}^{\infty} e^{ik_j^{II}(l+1/2)c}\sum_{\alpha=1}^{N_B} C_{j,mN_B+\alpha}^{II}|\mathbf{k}_\parallel, l; \alpha, II\rangle, \tag{B4}$$

where $r_{ij} = r(k_i^I \to k_j^I)$ is the reflection amplitude and $t_{ij} = t(k_i^I \to k_j^{II})$ is the transmission amplitude. k_j^I is a k_z solution (in general complex) of $E = E(\mathbf{k}_\parallel, k_z)$ for bulk material I with the negative group velocity if it is real or with $\mathrm{Im}(k_j^I) > 0$ if it is complex.[42] On the other hand, a k_z solution for material II, k_j^{II} must have either a positive group

velocity (if real) or $\mathrm{Im}(k_j^{II}) < 0$ (if complex). The evanescent states decay exponentially away from the interface and the change of the density of states in material I is mainly due to the states with real k_z unless the spacer is very thin and the imaginary part of k_z for the evanescent state is very small. At the interface, all evanescent states should be included to satisfy the boundary conditions. Boundary conditions are obtained by imposing $\langle \mathbf{k}_\parallel, l; \alpha | (H - E) | \psi_i \rangle = 0$ for $l = -m, \ldots, m-1$. These can be expressed in matrix forms. We define matrices B_1 and B_2 as

$$B_1 = \begin{pmatrix} 0 & 0 & -H_I^{(+2)} & 0 \\ 0 & 0 & -H_I^{(+1)} & -H_I^{(+2)} \\ H_{II,I}^{(-2)} & H_{II,I}^{(-1)} & 0 & 0 \\ 0 & H_{II,I}^{(-2)} & 0 & 0 \end{pmatrix},$$

$$B_2 = \begin{pmatrix} 0 & 0 & H_{I,II}^{(+2)} & 0 \\ 0 & 0 & H_{I,II}^{(+1)} & H_{I,II}^{(+2)} \\ -H_{II}^{(-2)} & -H_{II}^{(-1)} & 0 & 0 \\ 0 & -H_{II}^{(-2)} & 0 & 0 \end{pmatrix}. \tag{B5}$$

The average is taken for the matrix $H_{I,II}^{(\sigma)}$ or $H_{II,I}^{(\sigma)}$ at the interface and this is a good approximation when two materials have similar TB parameters such as Co and Cu. Using the eigenvectors of the companion matrix, we construct matrices Q_1 and Q_2 as

$$\begin{aligned} Q_1 &= (e^{\frac{1}{2}ik_1^I c} C_1^I, e^{\frac{1}{2}ik_2^I c} C_2^I, \ldots, e^{\frac{1}{2}ik_{N_A/2}^I c} C_{N_A/2}^I, 0, \ldots, 0), \\ Q_2 &= (0, \ldots, 0, e^{\frac{1}{2}ik_1^{II} c} C_1^{II}, e^{\frac{1}{2}ik_2^{II} c} C_2^{II}, \ldots, e^{\frac{1}{2}ik_{N_A/2}^{II} c} C_{N_A/2}^{II}), \end{aligned} \tag{B6}$$

where 0 is a null column vector. A is a column vector which consists of reflection and transmission amplitudes such that

$$A^t = (r_{i1}, r_{i2}, \ldots, r_{i,N_A/2}, t_{i1}, t_{i2}, \ldots, t_{i,N_A/2}), \tag{B7}$$

where A^t denotes the transpose of A. Then, the boundary conditions can be expressed as

$$B_1 e^{\frac{1}{2}ik_i^I c} C_i^I + (B_1 Q_1 + B_2 Q_2) A = 0. \tag{B8}$$

The reflection and transmission amplitudes which appear in A can be easily obtained from the above equation.

[1] P. Grünberg, R. Schreiber, Y. Pang, M. B. Brodsky, and H. Sowers, Phys. Rev. Lett. **57**, 2442 (1986).

[2] S. S. P. Parkin, N. More, and K. P. Roche, Phys. Rev. Lett. **64**, 2304 (1990).

[3] P. Bruno and C. Chappert, Phys. Rev. Lett. **67**, 1602 (1991); Phys. Rev. B **46**, 261 (1992).

[4] D. M. Edwards, J. Mathon, R. B. Muniz, and M. S. Phan, Phys. Rev. Lett. **67**, 493 (1991); J. Phys. Condens. Matter **3**, 4941 (1991).

[5] M. T. Johnson, S. T. Purcell, N. W. E. McGee, R. Coehoorn, J. aan de Stegge, and W. Hoving, Phys. Rev. Lett. **68**, 2688 (1992).

[6] M. T. Johnson, R. Coehoorn, J. J. de Vries, N. W. E. McGee, J. aan de Stegge, and P. J. H. Bloemen, Phys. Rev. Lett. **69**, 969 (1992).

[7] S. N. Okuno and K. Inomata, Phys. Rev. Lett. **70**, 1711 (1993).

[8] S. S. P. Parkin, C. Chappert, and F. Herman, Europhys. Lett. **24**, 71 (1993).

[9] J. F. Bobo, L. Hennet, and M. Piecuch, Europhys. Lett. **24**, 139 (1993); J. F. Bobo, L. Hennet, M. Piecuch, and J. Hubsch, J. Phys. Condens. Matter **6**, 2689 (1994).

[10] J. Unguris, R. J. Celotta, and D. T. Pierce, J. Magn. Magn. Mater. **127**, 205 (1993).

[11] J. Unguris, R. J. Celotta, and D. T. Pierce, J. Appl. Phys. **75**, 6437 (1994).

[12] M. D. Stiles, Phys. Rev. B **48**, 7238 (1993).

[13] J. Unguris, R. J. Celotta, and D. T. Pierce, Phys. Rev. Lett. **67**, 140 (1991).

[14] D. T. Pierce, J. A. Stroscio, J. Unguris, and R. J. Celotta, Phys. Rev. B **49**, 14 564 (1994).

[15] M. van Schilfgaarde and W. A. Harrison, Phys. Rev. Lett. **71**, 3870 (1993).

[16] E. E. Fullerton, M. J. Conover, J. E. Mattson, C. H. Sowers, and S. D. Bader, Phys. Rev. B **48**, 15 755 (1993).

[17] See, for example, A. R. Mackintosh and O. K. Andersen, in *Electrons at the Fermi Surface*, edited by M. Springford (Cambridge University Press, Cambridge, England, 1980).

[18] P. Lang, L. Nordström, R. Zeller, and P. H. Dederichs, Phys. Rev. Lett. **71**, 1927 (1993).

[19] L. Nordström, P. Lang, R. Zeller, and P. H. Dederichs, Phys. Rev. B **50**, 13 058 (1994).

[20] J. Kudrnovský, V. Drchal, I. Turek, and P. Weinberger, Phys. Rev. B **50**, 16 105 (1994).

[21] P. Bruno, J. Magn. Magn. Mater. **121**, 248 (1993); Europhys. Lett. **23**, 615 (1993).
[22] J. Mathon, M. Villeret, and D. M. Edwards, J. Magn. Magn. Mater. **127**, L261 (1993).
[23] The definition of v_{ij}^{α} and κ_{ij}^{α} is different from Ref. 12 by a factor of 2. For the free-electron case, $v_{ij}^{\alpha} = \hbar k_F/m$ and $\kappa_{ij}^{\alpha} = k_F$, where k_F is the Fermi wave vector and m is the electron mass.
[24] Z. Zhang, L. Zhou, P. E. Wigen, and K. Ounadjela, Phys. Rev. Lett. **73**, 336 (1994).
[25] Y.-C. Chang and J. N. Schulman, Phys. Rev. B **25**, 3975 (1982).
[26] D. A. Papaconstantopoulos, *Handbook of the Band Structure of Elemental Solids* (Plenum, New York, 1986).
[27] M. R. Halse, Philos. Trans. R. Soc. London, Ser. A **265**, 507 (1969).
[28] V. L. Moruzzi, J. F. Janak, and A. R. Williams, *Calculated Electronic Properties of Metals* (Pergamon, New York, 1978).
[29] K. Garrison, Y. Chang, and P. D. Johnson, Phys. Rev. Lett. **71**, 2801 (1993); C. Carbone, E. Vesocovo, O. Rader, W. Gudat, and W. Eberhardt, *ibid.* **71**, 2805 (1993).
[30] P. J. H. Bloemen, R. van Dalen, W. J. M. de Jonge, M. T. Johnson, and J. aan de Stegge, J. Appl. Phys. **73**, 5972 (1993).
[31] Z. Q. Qiu, J. Pearson, and S. D. Bader, Phys. Rev. B **46**, 8659 (1992).
[32] Their result is the energy difference of the ferromagnetic and antiferromagnetic configuration and divided by two in order to be consistent with our definition.
[33] M. van Schilfgaarde and F. Herman, Phys. Rev. Lett. **71**, 1923 (1993).
[34] A. Rabe, N. Memmel, A. Steltenpohl, and Th. Fauster, Phys. Rev. Lett. **73**, 2728 (1994).
[35] W. F. Egelhoff, Jr. and M. T. Kief, Phys. Rev. B **45**, 7795 (1992).
[36] A. Schreyer, K. Bröhl, J. F. Ankner, C. F. Majkrzak, Th. Zeidler, P. Bödeker, N. Metoki, and H. Zabel, Phys. Rev. B **47**, 15 334 (1993).
[37] S. S. P. Parkin, R. Bhardra, and K. P. Roche, Phys. Rev. Lett. **66**, 2152 (1991).
[38] D. H. Mosca, F. Petroff, A. Fert, P. A. Schroeder, W. P. Pratt, Jr., and R. Laloee, J. Magn. Magn. Mater. **94**, L1 (1991).
[39] Since our results are for the asymptotic behavior, the trend may be somewhat different from the experimental data which correspond to the first antiferromagnetic peaks.
[40] J. d'Albuquerque e Castro, M. S. Ferreira, and R. B. Muniz, Phys. Rev. B **49**, 16 062 (1994).
[41] J. C. Slater and G. F. Koster, Phys. Rev. **94**, 1498 (1954).
[42] For the real k_z, it is the solution of $E(k_z)+i\delta = 0$ ($\delta \to +0$) in the upper half complex k_z plane.